Surface contact charging

Troy Shinbrot,[1,2,*] Matthew Rutala,[1] and Hans Herrmann[3]
[1]*Department of Biomedical Engineering, Rutgers University, Piscataway, New Jersey 08854, USA*
[2]*Princeton University, Princeton, New Jersey 08544, USA*
[3]*ETH, Stefano-Franscini-Platz 5, CH-8049 Zürich, Switzerland*
(Received 1 June 2017; published 22 September 2017)

Experiments in several laboratories have demonstrated that identical materials brought into repeated contact generate unexplained and growing surface charge domains. Here we show that the growth of charge from these experiments can be fitted to a previously developed first-principles model for contact charging based on feedback of random surface polarizations. Surprisingly this mechanism, which leads to exponential growth in colliding granular beds, can also explain nonexponential growth of surface charging, as well as predicting spatiotemporal growth of charge domains and their dependencies on material parameters.

DOI: 10.1103/PhysRevE.96.032912

I. BACKGROUND

Anyone who has looked under a couch knows how assiduously dust can spread and adhere to surfaces. The motion and sticking of particles is not limited to tiny motes of dust: rubbing a balloon against your hair—or even against another balloon—will generate enough charge to make it stick to a wall. Merely a curiosity at home, particle charging is a serious issue. Faraday himself was hired to investigate a mine explosion that killed 95 men and boys; among his findings were that thick layers of flammable coal dust adhered to surfaces near the explosion [1]. Technologically, a high point in the field was the invention of the photocopier by Carlson who had the idea—rejected by consultants as pointless—that charged particles could be used to form a permanent image on paper [2].

So how do particles—or more generally surfaces—charge? In view of the ongoing and historic nature of the problem, an observer would be forgiven for believing that the question has been answered, however even charging material as commonplace as a child's balloon is not easily explained [3,4]. An essential issue in the field is that several laboratories have demonstrated that identical materials charge one another after symmetric contact. In Fig. 1, we summarize these results, showing that identical balloons in sliding contact [5], identical polycarbonate disks in rolling contact [5], and silicone sheets in normal contact [6] all break symmetry and charge one another. In these panels, we reproduce voltage and charge plots showing that the quantitative charging in the three experiments appears to behave similarly. In this paper, we analyze this problem and show that this charging behavior is reproduced using a recently described first-principles model [7–10]. We show fits of this model to the three experiments in each panel of Fig. 1.

We propose that the essential physics of contacting surfaces can be described by two lattices of identical dielectric particles that are periodically brought into near contact. Modeling approaches have been presented previously [7–10]; in the present work, each particle has the same radius, R, and is fixed in a close-packed hexagonal lattice as depicted in Fig. 2(a). We embed two charges within every particle, each located $\frac{3}{4}R$ from the particle center. The magnitudes and angular locations of the charges depend on the applied field (to mimic charge induction) and contact between upper and lower lattices (to mimic charge neutralization). In this way, as sketched in Fig. 2(b), if the two charges on particle i are q_{i1} and q_{i2}, then the particle will possess a net charge $q_{i1}+q_{i2}$, and a polarization $(q_{i1}-q_{i2})\vec{r}$, where $\vec{r}$ is the vector connecting the charges, and $|\vec{r}|=\frac{3}{2}R$.

Evolution of charges is defined as a discrete time mapping, where each time increment represents one cycle of bringing the separated surfaces into and then out of contact. So if particle i at time t has a polarization $p_i(t)$, then at time $t+1$, it will acquire polarization $\vec{p}_i(t+1)$ given by the vector sum $\vec{p}_i(t)+\vec{p}_i^{\,\mathrm{ind}}$. The induced polarization, $\vec{p}_i^{\,\mathrm{ind}}$, is assumed to simply be proportional to the electric field due to charges on the opposing surface,

$$\vec{p}_i^{\,\mathrm{ind}} = \alpha \sum \vec{E}_j \tag{1}$$

as sketched in Fig. 2(a). Here α is a constant polarizability and $\sum \vec{E}_j$ is the electric field due to all particles on the opposing surface. Only the opposing surface is used for this calculation because particles on either surface do not move with respect to one another, and the energy required to change a particle's polarization is considered to be done by the work of moving the surfaces—and their embedded charges—relative to one another. In principle charges on a particle's own surface also contribute to induced polarization, but no work is done—and so no charge separation is produced—by this polarization, and so it is neglected in our calculations of surface charge evolution.

We calculate $\vec{E}_j$ at a fixed separation between surfaces [ΔZ in Fig. 2(a)]. This separation is intended to account for the fact that real surfaces (as in the experiments of Fig. 1) are seldom atomically flat but have surface imperfections and asperities.

After polarization has been induced according to Eq. (1), neutralization is imposed by requiring the vector component of the charges on adjacent contacting surfaces to obey

$$\begin{aligned} \hat{q}_i &\rightarrow \tfrac{1}{2}[\hat{q}_i\,(2-\eta)+\hat{q}_j\,\eta], \\ \hat{q}_j &\rightarrow \tfrac{1}{2}[\hat{q}_i\,\eta+\hat{q}_j\,(2-\eta)], \end{aligned} \tag{2}$$

*shinbrot@rutgers.edu

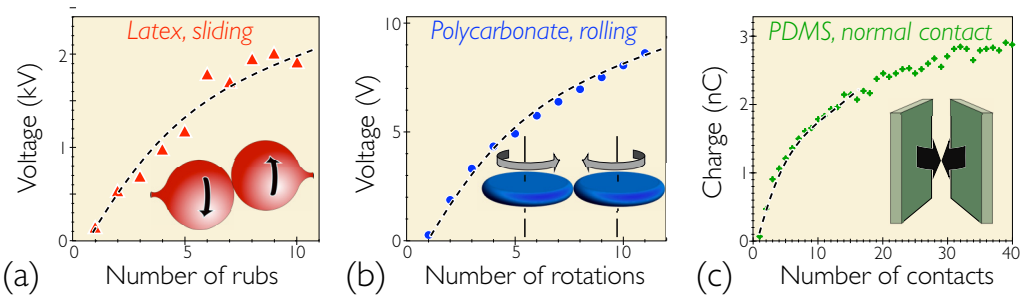

FIG. 1. Spontaneous charging of identical materials in three experiments. (a) Latex balloons slid symmetrically in circular motions against one another as indicated in inset, with charging measured using a noncontact voltage probe at a fixed distance after each circuit of motion; (b) polycarbonate disks in symmetric rolling contact, with charging measured using a different noncontact probe after each rotation; (c) virgin PDMS sheets in symmetric normal contact, with charging measured using an electrometer and Faraday cup after each contact. Data in panels (a) and (b) are from Ref. [5], and data in panel (c) are from Ref. [6]. Broken lines show comparison with model described in text and shown also in Fig. 3(d).

where η is a neutralization efficiency, and as indicated in Fig. 2(b), $\hat{q}_i$ is the fraction of charge that faces downward on the ith particle on the top surface, and $\hat{q}_j$ is the fraction of charge that faces upward on the nearest particle beneath. Explicitly, $\hat{q}_i = q_{i(1,2)}\cos(\varphi_i)$, where φ_i is the polar angle of the polarization vector $\vec{r}_i$ shown in Fig. 2(b). In this way, if $\vec{r}_i$ were pointing vertically, φ_i would be 0, and $\hat{q}_i$ would be whichever charge is facing the interface between surfaces (denoted $q_{i(1,2)}$), while if $\vec{r}_i$ were pointing off of vertical, then the nearest charge would be decomposed into a vertical and a nonvertical component, and only the vertical component would participate in neutralization.

As for the neutralization efficiency, when $\eta = 0$, Eq. (2) leaves contacting charges unchanged, and when $\eta = 1$, Eq. (2) reduces to the average charge, $(q_i + q_j)/2$. Charge is explicitly conserved by both Eqs. (1) and (2): the total charge on each particle is constant during induction, and the charge of pairs of particles is constant during neutralization.

In previous work [7–10], it was demonstrated that the mechanism of repeated polarization and neutralization defined by Eqs. (1) and (2) leads to exponential growth in charging. This occurs because the electric field defined by Eq. (1) grows multiplicatively with the polarization: a straightforward recipe for exponential growth. In this paper we show that the same mechanism can unexpectedly lead to transient growth in surface charging that differs from this recipe in significant ways.

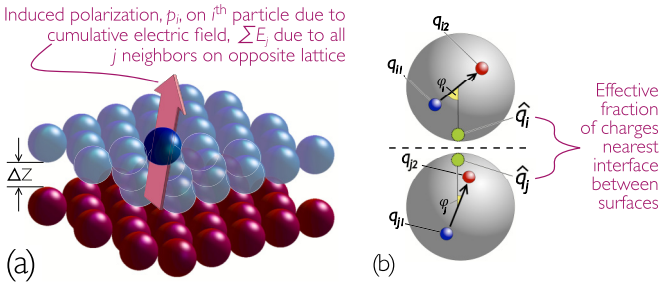

FIG. 2. Illustrations of charging mechanism. (a) Induction defined by Eq. (1): two parallel hexagonal lattices of particles, where the electric field on every particle is calculated by summing the fields due to all particles on the opposing lattice. The dark particle is an exemplar in the upper lattice whose induced polarization is as shown. Colors here are only used to distinguish upper from lower lattices. (b) Neutralization defined by Eq. (2): every particle in each lattice contains two charges: q_{i1}, q_{i2} in particle i, and q_{j1}, q_{j2} in particle j. Blue here indicates negative, and red positive, charges. The effective fractions of the charges $\hat{q}_i$ and $\hat{q}_j$ nearest the interface between the surfaces are defined geometrically as described in the text, and these charges neutralize according to Eq. (2).

We present results of this model next, but before doing so we stress two caveats. First, as with any model, it is only an approximation. It does not describe the microscopic chemistry or physics of how charges rearrange to produce the phenomenological behaviors defined by Eqs. (1) and (2). Several groups have published important contributions, for example dealing with changes to effective material work functions due to the fields produced by charged particles [11–13], and with carriers that may be responsible for surface charge transport [14,15]. Second, the change in polarization on a particle inevitably feeds back on itself; i.e., the field from a polarized particle induces a polarization on other particles that in turn affect the original particle's polarization. In prior work [16], we have shown that this feedback converges rapidly; e.g., the error compared with the asymptotic state is typically under 0.8% after 2 iterations of polarization calculation. We therefore use 3 iterations in our calculations, but we note that more rapid convergence has also been shown to be possible [17].

II. HIGH-NEUTRALIZATION RESULTS

To explore the charging of surfaces, we perform simulations in which Eqs. (1) and (2) are sequentially and repeatedly applied to two close-packed hexagonal lattices of 50×50 identical particles, where the lattices are separated by $\Delta Z = 1$ particle diameter [as indicated in Fig. 2(a)]. Available data (Fig. 1) are produced in experiments in which contact times between surfaces range from 1 second to over an hour [6], and so we assume that there is ample time for complete neutralization to occur. Thus we start with the case where the neutralization efficiency is 100% [$\eta = 1$ in Eq. (2)]. This differs from earlier simulations [7–10] of collisional grains in which contact times are short, and so for completeness we follow this first simulation with additional simulations in which we investigate the effect of varying η.

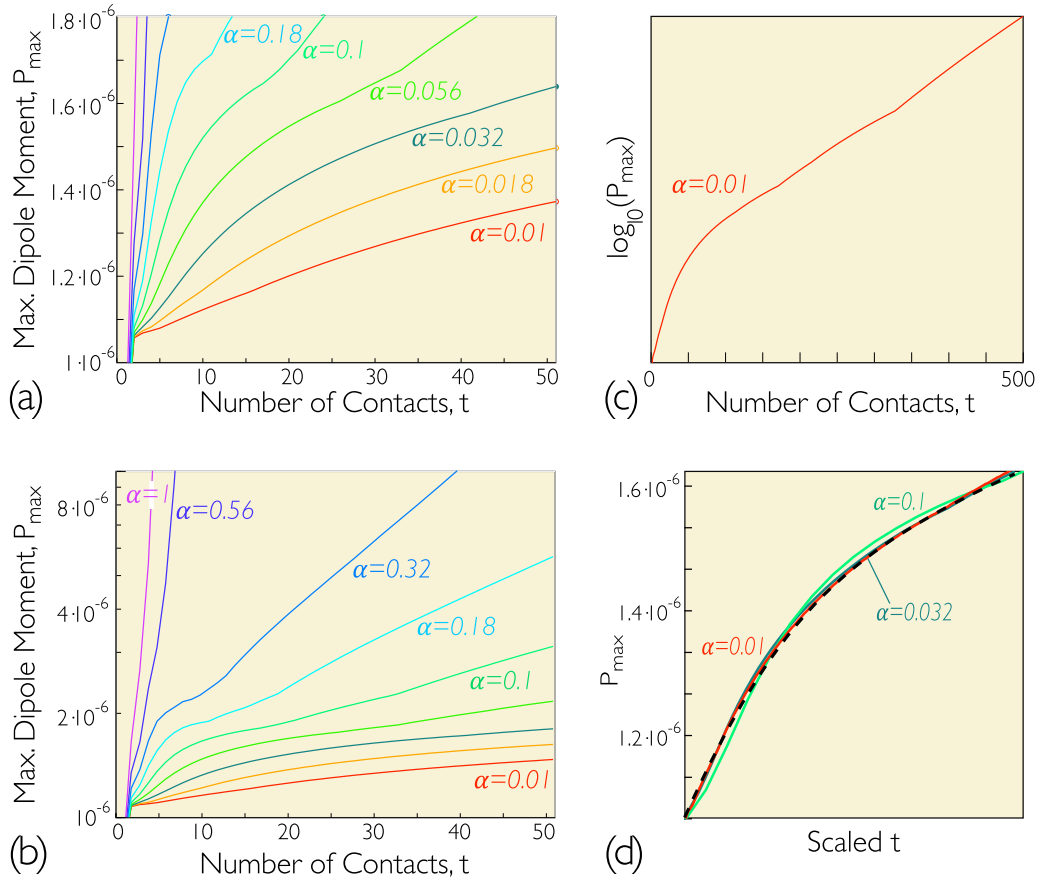

FIG. 3. Simulation results. (a) Maximum dipole moment evaluated over lattices of 50 × 50 particles vs number of contacts under application of Eqs. (1) and (2) for polarizabilities, α, indicated. Surface asperities are modeled by taking contact to occur when arrays are $\Delta Z = 1$ diameter apart [ΔZ shown in Fig. 2(a)]. (b) The same plot as in (a) on a semilog scale: note exponential growth occurs after an initial concave-down transient. (c) $\alpha = 0.01$ case extended to 500 contacts, showing exponential growth after long times. (d) Concave-down regimes scale: here we display linear plots of three exemplars where t is multiplied by a constant scale factor to produce data collapse. Broken curve is overlaid on data from each of the existing experiments in Figs. 1(a)–1(c).

Particles are initialized with small random charges. Explicitly, each particle is initially neutral, with two charges $q_{i1} = -q_{i2}$ chosen from a uniform distribution on $[-10^{-6}, 10^{-6}]$, and with unit vector $\vec{r}/|\vec{r}|$ connecting the charges chosen with random azimuthal and polar angles. In Fig. 3(a), we show the magnitude of the maximum dipole moment, $P_{\max} \equiv \max(\vec{p}_{i,j})$, among the 50 × 50 pairs of particles for polarizabilities ranging from $\alpha = 0.01$ to $\alpha = 1$.

We calculate the maximum rather than the another measure (e.g., the mean of absolute values, $\langle|q_{i,j}|\rangle$) both to provide an unambiguous measure of the fastest growth in a lattice and to facilitate comparison with prior work [7–10]. Asymptotically, the fastest growing charges dominate the mean and so the two measures produce the same results. Transient growth, on the other hand, is systematic and predictable when evaluated using $P_{\max}$, however we have found that measures such as $\langle|q_{i,j}|\rangle$ can vary erratically as charge domains migrate, compete, and annihilate.

Plots in Fig. 3(a) are on a linear scale, and evidently the growth in polarization is concave down for all cases: qualitatively similar to what is seen in experiments (Fig. 1), and distinct from the exponential growth reported elsewhere [7–10].

We note that the direction of concavity can change on a semilog scale for growth that is slower than exponential, and if we instead plot the same data on semilog axes, we obtain the result shown in Fig. 3(b), where we see both a concave-down regime for shorter times, and an exponential regime at longer times. This is most visible here for the case $\alpha = 0.32$, but longer trials confirm that this is a general result for all polarizabilities; for example in Fig. 3(c), we show an exponential regime for $\alpha = 0.01$, which appears after about 100 contacts.

We investigate the cause of nonexponential transient growth next, but first we observe that for all α, linear plots of the transient regime can be collapsed by simple scaling: *scaled* $t = \omega_\alpha t$, where the constant ω_α is found empirically to be 22 ± 1. In Fig. 3(d), we show three examples of this scaling, and we also overlay the black curve from this plot as a broken line alongside experimental data in Fig. 1. In that figure, the broken line only represents the curve in the region of data collapse shown in Fig. 3(d). Depending on polarizability, α, used in experiments, charges may grow exponentially outside of this region [as shown in Figs. 3(b) and 3(c)], or may grow more slowly [as shown in Fig. 3(a)]. Thus the comparison shown in Fig. 1 is not definitive; nevertheless it suggests that

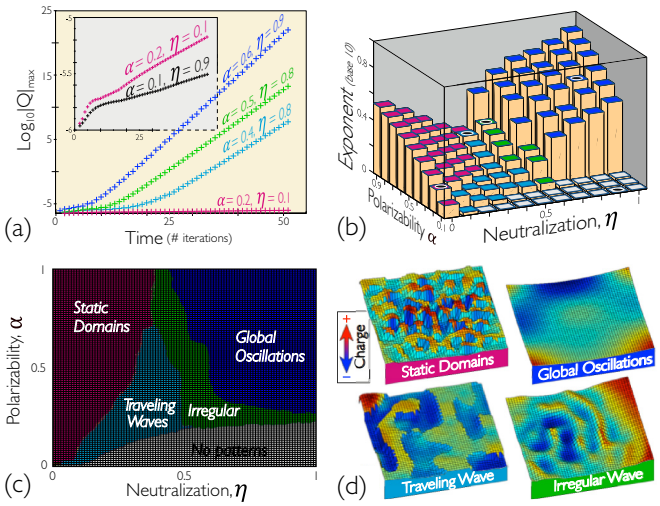

FIG. 4. Charging behaviors of 50 × 50 2D lattice model. (a) Exemplars showing exponential growth of magnitudes of maximum charges on lattice. Exponential growth of slowly charging examples is not obvious, so in the inset, we expand the semilog scale in two such cases. (b) Exponential rates of growth (after transient of 32 time steps) of largest polarization, $P_{\max}$, as a function of polarizability, α, and neutralization, η. Color coding distinguishes patterns observed, and black spots identify cases shown in panel (a). (c) Patterns expressed as α and η are varied in 0.01 increments; color coding as in panel (b). (d) Snapshots of net charge magnitudes on upper surface after 50 time steps. Static domains are steady; the other states fluctuate in time (also shown in the videos in the Supplemental Material [22]). Color coding according to charge on logarithmic scale (i.e., red value $= +\log_{10}|P_{\max}|$, blue value $= -\log_{10}|P_{\max}|$; see text).

a mechanism such as we have described may be involved in surface charging.

III. CHARGING VERSUS POLARIZABILITY AND NEUTRALIZATION

To better understand the mechanisms underlying contact charging, we vary the polarizability, α, from 0.1 to 0.9, and the neutralization, η, from 0 to 1, in the model that we have defined. As illustrated in Fig. 4(a) through several exemplars at broadly ranging choices of α and η, we find that charge growth is invariantly exponential for sufficiently many repetitions of contact. Despite this apparent similarity, qualitatively different patterns of charging—both in time and in space—are seen as α and η are varied.

This is apparent by considering Fig. 4(b), where we plot exponents of growth obtained in the exponential regime (for times >32). Here we see a systematic confirmation first that most choices of α and η produce asymptotically exponential growth rates, and second that distinct regimes of exponential growth are identifiable. As we will describe, these distinct regimes of growth rates are correlated with distinct spatial patterns of growth.

In Fig. 4(c), we identify these spatial patterns in a more detailed phase diagram. Here we have performed multiple simulations at increments of 0.01 in both α and η and at varying time scales (between 50 and 500 iterations, until an asymptotic spatial pattern was obtained). We found four distinct patterns [shown as snapshots in Fig. 4(d)] as follows.

For small η [magenta in Figs. 4(c) and 4(d)] we observe an irregular static array of positively and negatively polarized domains. We will discuss this pattern in more detail shortly, but in overview, domains attain a fixed polarization direction early in the simulation, and consolidate thereafter. There is some jockeying for position during a transient period, and for larger α charges grow more rapidly, but essentially the strongest domains establish themselves early and grow in strength—though not in size—thereafter. We have remarked that both polarization [Eq. (1)] and neutralization [Eq. (2)] mechanisms are charge conserving, and consequently the number, size, and magnitude of positively and negatively charged domains are comparable.

For small α on the other hand, individual dipoles correlate little with their neighbors, and no spatial patterns are perceptible. This makes sense since α is the measure of neighbor-neighbor induction, and as $\alpha \to 0$, spatial correlation should vanish. Growth is substantially slower than at larger values of α, but nevertheless growth becomes exponential at longer times: this is shown in the inset to Fig. 4(a), where we also include a typical case of slow growth without a spatial pattern, at $\alpha = 0.1,\ \eta = 0.9$. As expected, the iterative nature of the charging mechanism described leads asymptotically to exponential growth for any nonzero α.

At the other extreme, at large α and η, we encounter global oscillations. The mechanism for the emergence of this state can be understood by observing that at large η, the charges nearest the contacting surface (nearly) neutralize, and only outermost charges, farthest from that surface, remain [sketched in Fig. 5(a)]. Those residual outermost charges grow multiplicatively after repetition of Eq. (1), and these charges must be of opposite sign, else charge would not be conserved. For strong neutralization but weak polarizability, the residual charges diminish in magnitude as depicted in Fig. 5(b); however for strong polarizability, the induced charges can in principle exceed the magnitude of the existing charges, which causes the ultimate charges to reverse in sign. This case is depicted in Fig. 5(c), and results in the two outermost charges switching signs every time step as they increase in magnitude, which is what we see in simulations.

Between the extremes of η and α, we find wavelike states as indicated in Figs. 4(c) and 4(d). We term these states "traveling" and "irregular" waves [22]. Traveling waves move smoothly and continuously, while irregular waves are instantaneously similar, but rapidly switch sign. We interpret the changes in sign as being due to high η and α, as described in Figs. 5(a)–5(c).

Apparently, as shown in Fig. 5, simple geometrical arguments can be used to analyze charging mechanisms, so for strong polarization and neutralization, outermost surfaces attain opposite charges that globally coordinate and switch signs every time step. Geometrical arguments also provide insights into the static domain configuration shown in Fig. 4. In Fig. 6(a), we show a typical plan view of charges, using a logarithmic color map. The arrangement of domains is never quite regular; nevertheless, charge patterns obey clear geometrically based rules.

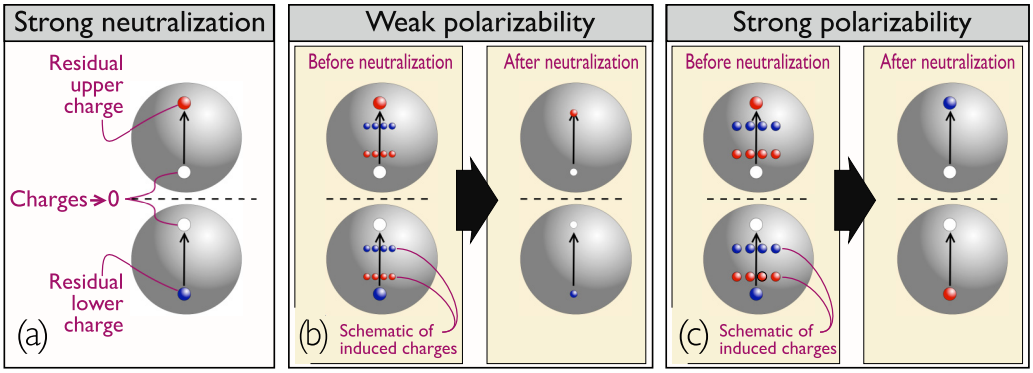

FIG. 5. Charging at large η and α. (a) For large η, contacting charges neutralize, leaving residual charges on surfaces farthest from contact. These residual charges dominate the resulting dynamics. (b) For large η and small α, induction produces polarization charges (sketched at left of panel) that reduce the residual charge magnitudes (as shown at right of panel). (c) For large η and large α, the induced charges can exceed the original charges, and the residual charge therefore changes sign every time step.

To understand these rules, note as shown at the left of Fig. 6(b) that two dipoles oriented normal to the contact plane will tend to align in parallel, so that negative and positive charges are adjacent. The antiparallel orientation is unstable, as that would place like charges, which repel, nearby one another. By the same reasoning, if the dipoles are oriented in the contact plane, as shown at the right of Fig. 6(b), the *parallel* orientation is unstable, for again this would place like charges nearby. Instead, such dipoles orient either antiparallel, as shown in Fig. 6(b), or in-plane, but skewed with respect to one another (not shown). In Fig. 6(c), we provide a quiver plot of upper (blue) and lower (green) dipole unit vectors (i.e., all vector magnitudes are plotted as being constant), and we identify parallel and antiparallel dipoles that obey the rule described in Fig. 6(b). Examples of skew dipoles can also be found, but are not identified here.

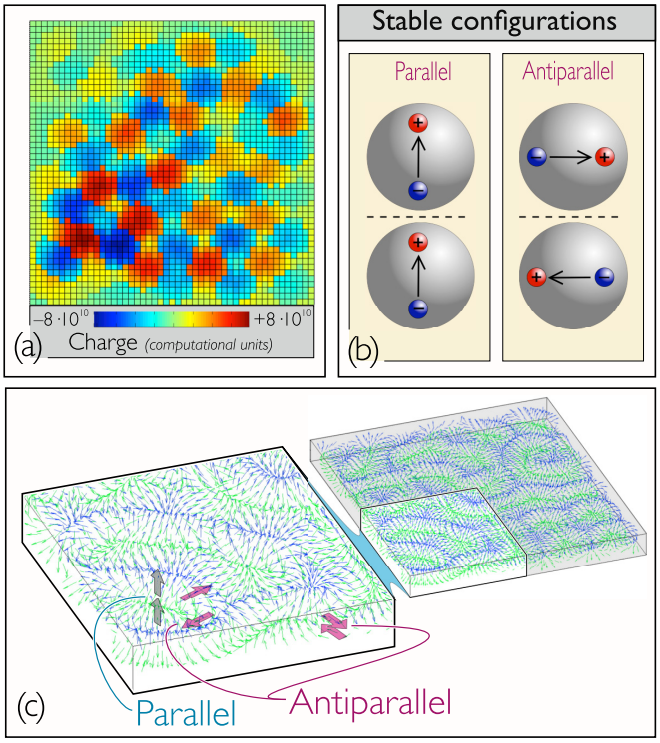

FIG. 6. Static domain pattern at $\eta = 0.8$, $\alpha = 0.2$. (a) Charge magnitudes (colors on logarithmic scale). (b) At the center of each colored spot, dipoles are oriented perpendicular to the contact plane, and upper and lower dipoles are parallel. Between these spots, dipoles are oriented in the contact plane, in which case positive charges align with negative ones in an antiparallel configuration. (c) Parallel and antiparallel orientations are identified in quiver plot of the same simulation as in panel (a). Green quivers are in the lower lattice; blue are in the upper.

IV. CONCLUSION

It has been known at least since the 16th century that insulating materials charge more readily than conducting ones [18], and for over 30 years that identical materials can tribocharge one another [19]. The mechanism by which insulators recruit charge carriers, or by which identical insulators break symmetry to choose charged states, has only recently been investigated.

In the present work, we have shown that aspects of existing data of the charging of surfaces can be explained by focusing on dipoles rather than on net charges. Indeed, by the same token that it is mysterious that net charges of opposite signs build in proximity to one another, it is entirely predictable that dipoles do so. Likewise, only in insulators can the mutual reinforcement of nearby dipole moments occur. And as we have shown, if the nearest parts of mutually reinforcing dipoles neutralize, a self-consistent, charge-conserving first-principles model can be constructed that appears to agree with existing experimental data.

In particular, in the limit of long contact times between surfaces—and so high neutralization efficiencies—we find that all experimental data, shown in Fig. 1, collapse onto a master curve, as shown in Fig. 3(d). Further, we predict that localized charge domains should be seen for high polarizability and low neutralization (e.g., on pristine, high dielectric constant surfaces [6]), while as neutralization efficiency grows (e.g., through surface contamination by water or other mediators of charge transport [14,15]), spatiotemporal states should emerge. Existing data (Fig. 1) seem to generate steady, or nearly steady, charge growth, and more detailed experiments

will be needed to determine whether such spatiotemporal states in fact occur.

The simplified simulations that we have presented here beg the question of how, in detail, surface transport of charge interacts with polar molecules in bulk insulators [20]. This is a fundamental question that will require intensive research to resolve in the future. Our results so far suggest that the underlying practical finding—in dissimilar as well as identical insulators—should be that growth of localized charge domains is the rule, and that this growth should asymptotically be exponential, though slower transient growth can also occur. Moreover, our results indicate that the well-known lack of reproducibility of tribocharging [3,21] may be the result of an intrinsic exponential growth mechanism that amplifies infinitesimal imperfections, and not due to lack of experimental care, as has long been believed.

ACKNOWLEDGMENTS

This material is based on work supported by the US National Science Foundation under Grant No. 1404792. We thank the European Research Council (ERC), Advanced Grant No. 319968-FlowCCS, for financial support.

[1] M. Faraday and C. Lyell, Report to the Home Secretary on the explosion at the Haswell colliery on 28 September 1844, Philos. Mag. **26**, 16 (1845).

[2] D. Owen, *Copies in Seconds: Chester Carlson and the Birth of the Xerox Machine* (Simon & Schuster, New York, 2004).

[3] D. J. Lacks and R. M. Sankaran, Contact electrification of insulating materials, J. Phys. D **44**, 453001 (2011).

[4] L. B. Schein, Recent progress and continuing puzzles in electrostatics, Science **316**, 1572 (2007).

[5] T. Shinbrot, T. S. Komatsu, and Q. Zhao, Spontaneous tribocharging of similar materials, Europhys. Lett. **83**, 24004 (2008).

[6] M. M. Apodaca, P. J. Wesson, K. J. M. Bishop, M. A. Ratner, and B. A. Grzybowski, Contact electrification between identical materials, Angew. Chem., Int. Ed. **49**, 946 (2010).

[7] T. Siu, J. Cotton, G. Mattson, and T. Shinbrot, Self-sustaining charging of identical colliding particles, Phys. Rev. E **89**, 052208 (2014).

[8] R. Yoshimatsu, N. A. M. Araújo, G. Wurm, H. J. Herrmann, and T. Shinbrot, Self-charging of identical grains in the absence of an external field, Sci. Rep. **7**, 39996 (2017).

[9] T Pähtz, H. J. Herrmann, and T. Shinbrot, Why do particle clouds generate electric charges?, Nat. Phys. **6**, 364 (2010).

[10] R. Yoshimatsu, N. A. M. Aruajo, T. Shinbrot, and H. J. Herrmann, Field driven charging dynamics of a fluidized granular bed, Soft Matter **12**, 6261 (2016).

[11] J. Kolehmainen, A. Ozel, C. M. Boyce, and S. Sundaresan, Triboelectric charging of monodisperse particles in fluidized beds, AIChE J. **63**, 1872 (2017).

[12] J. C. Laurentie, P. Traoré, and L. Dascalescu, Discrete element modeling of triboelectric charging of insulating materials in vibrated granular beds, J. Electrostatics **71**, 951 (2013).

[13] T. Matsusyama and H. Yamamoto, Impact charging of particulate materials, Chem. Eng. Sci. **61**, 2230 (2006).

[14] L. S. McCarty and G. M. Whitesides, Electrostatic charging due to separation of ions at interfaces: Contact electrification of ionic electrets, Angew. Chem., Int. Ed. **47**, 2188 (2008).

[15] R. Fu, X. Z. Shen, and D. J. Lacks, First principles study of the charge distributions in water confined between dissimilar surfaces and implications in regard to contact electrification, J. Phys. Chem. C **121**, 12345 (2017).

[16] T. Siu, W. Pittman, J. Cotton, and T. Shinbrot, Nonlinear granular electrostatics, Granular Matter **17**, 165 (2015).

[17] K. Barros, D. Sinkovits, and E. Luijten, Efficient and accurate simulation of dynamic dielectric objects, J. Chem. Phys. **140**, 064903 (2014).

[18] W. Gilbert, *De Magnete*, translated by P. Fleury Mottelay (J. Wiley & Sons, New York, 1991), p. 83.

[19] J. Lowell and W. S. Truscott, Triboelectrification of identical insulators. I. An experimental investigation, J. Phys. D **19**, 1273 (1986).

[20] M. Z. Hasan and C. L. Kane, Colloquium: Topological insulators, Rev. Mod. Phys. **82**, 3045 (2010).

[21] W. R. Harper, *Contact and Frictional Electrification* (Oxford University Press, Oxford, UK, 1967).

[22] See Supplemental Material at http://link.aps.org/supplemental/10.1103/PhysRevE.96.032912 for videos showing traveling and irregular waves.